



Examining the surface of a synergistic Pt-Rh/ γ -Al₂O₃ catalyst using NO as a probe molecule

Paul S. Dimick^{a,*}, John L. Kross^b, Erin G. Roberts^b, Richard G. Herman^c, Harvey G. Stenger^a, Charles E. Lyman^b

^a Lehigh University Department of Chemical Engineering, 111 Research Drive, Bethlehem, PA 18015, United States

^b Lehigh University Department of Materials Science and Engineering, 5 East Packer Avenue, Bethlehem, PA 18015, United States

^c Lehigh University Department of Chemistry, 6 East Packer Avenue, Bethlehem, PA 18015, United States

ARTICLE INFO

Article history:

Received 29 April 2008

Received in revised form 19 November 2008

Accepted 20 November 2008

Available online 27 November 2008

Keywords:

Nitric oxide probe molecule

Platinum–rhodium

Bimetallic nanoparticle

Surface segregation

Synergistic catalyst

ABSTRACT

The interaction of NO and NO + H₂ with reduced γ -Al₂O₃, Pt/ γ -Al₂O₃, Rh/ γ -Al₂O₃, Pt(90%)-Rh/(10%)/ γ -Al₂O₃ (90/10), and Pt(95%)-Rh(5%)/ γ -Al₂O₃ (95/5) was monitored with FTIR spectroscopy to better understand the surface of a synergistic Pt-Rh catalyst (95/5). The surface of the alloy nanoparticles on the synergistic 95/5 catalyst contained both Pt and Rh due to the presence of FTIR peaks representing linear NO on Pt and NO on Rh. The presence of Pt and Rh on the surface of 90/10 was confirmed through the observation of the linear NO-on-Pt peak and the Rh nitrosyl peak, respectively. The presence of the Rh nitrosyl peak at 150 °C and 200 °C on 90/10 indicates the presence of partially oxidized Rh on the surface of the supported Pt-Rh alloy particles at these temperatures. The following relative order of NO reduction activity was observed for the prepared catalysts: 95/5 > Pt/ γ -Al₂O₃ \approx 90/10 \gg Rh/ γ -Al₂O₃. The maximum synergistic performance of 95/5 was a five-fold increase over the activity of Pt/ γ -Al₂O₃, and this was only observed after conditioning the catalyst by equilibrating to reaction conditions for 10 h at 250 °C. A discussion of the reaction mechanism and the observed surface species reveals that the differing performance of 95/5 and 90/10 is related to the amount of Rh on the surface of the supported alloy nanoparticles.

© 2008 Elsevier B.V. All rights reserved.

1. Introduction

Recent air-pollution catalyst research has been focused on the development of effective lean-burn and nitrogen storage and reduction (NSR) catalysts using a variety of reductants including H₂, hydrocarbons, and alcohols [1–6]. Automotive air-pollution catalysts typically operate at temperatures between 400 °C and 800 °C [2], but catalysts that are active at low temperatures (<300 °C) are better suited for stationary source applications such as NO_x emissions abatement from coal-fired power plants. Platinum is often used in low-temperature NO reduction catalysts because of its high activity, while other metals such as Rh are less active but exhibit better selectivity towards N₂. Pt-Rh bimetallic catalysts have been shown to perform synergistically by several researchers for the NO/H₂, NO/CO, CO/O₂, and NO/CO/H₂ reactions [7–11]; however, other researchers did not observe this synergy [12,13]. Through a series of analytical electron microscopy (AEM) studies, Lakis and co-workers showed that a Pt(95%)-Rh(5%)/ γ -Al₂O₃ NO reduction catalyst behaved synergis-

tically because the catalyst consisted of a single phase of Pt-rich nanoparticles, while other compositions did not perform synergistically because both Pt-rich and Rh-rich particles were present [7,8,14–16].

It is well known that the effectiveness of a supported bimetallic catalyst depends on its surface composition which is a function of particle composition, degree of metal interaction, interaction between the metal particles and support, particle size, pretreatment conditions, and chemical state of the metals [7,8,11,17,18]. In the absence of a gas-phase atmosphere, the element with the lowest surface energy, Pt in the case of a Pt-Rh alloy [19], will segregate to the surface of the nanoparticle. Introducing a gas that strongly adsorbs to the element of higher surface energy can shift chemical equilibrium and bring the high-surface-energy element to the surface [20].

Several studies have been conducted on Pt-Rh single crystals to determine the effect of adsorbing NO, O₂, and H₂ on surface composition [21–27]. It has been shown that adsorbing NO or O₂ on single crystal Pt-rich and Rh-rich alloys and bimetallics results in the formation of a predictable, oxygen-covered, Rh-rich surface structure that depends on adsorption temperature and crystal orientation [22–27]. Catalytic activity measurements on these surfaces have shown that the restructured surface performs synergistically for the reduction of NO with H₂ compared to Pt

* Corresponding author. Tel.: +1 610 758 4237.

E-mail address: paulsdimick@gmail.com (P.S. Dimick).

and Rh single crystals [24–27]. Exposing the activated Pt–Rh–O surface to H_2 results in a surface reconstruction that brings Pt to the crystal surface; however, this surface reverts to the activated surface upon exposure to NO or O_2 , even at low temperatures [24–27]. Recently, NO- and O_2 -induced Rh surface segregation has also been observed with a three-dimensional atom probe in nanocrystalline Pt–Rh Field Ion Microscopy specimens [28–31].

It is also documented that the interaction of NO with monometallic supported Pt and Rh catalysts results in structural changes. A study by Bourane et al. [32] showed that high-temperature adsorption of NO on a Pt/ γ - Al_2O_3 catalyst results in the reconstruction of the surface of Pt particles as indicated by changes in the NO–Pt peaks observed with FTIR spectroscopy; these changes were irreversible until the catalyst was reduced. This phenomenon has also been observed for the adsorption of NO on Pt single crystals [33–36], and it has been postulated to arise from the dissociation of NO on the Pt surface [37]. Adsorption of NO on monometallic Rh catalysts can cause oxidative disruption of supported Rh nanoparticles [38,39]. It is important to consider that NO can adsorb both molecularly and dissociatively, which impacts the activity, selectivity, and surface structure of the catalysts [21,40–43]. Understanding the interaction of NO with supported Pt–Rh alloy nanoparticles is required to explain their synergistic performance for the NO/ H_2 reaction.

The present study compares the activity of two bimetallic catalysts with their monometallic counterparts for the reduction of NO with H_2 and then uses in situ FTIR spectroscopy to qualitatively examine the surface species present when they interact with NO and NO + H_2 . Only one bimetallic is found to be synergistic. The interaction of NO with γ - Al_2O_3 -supported monometallic and bimetallic catalysts containing Pt and Rh with and without the presence of O_2 and various organic reductants are well documented [18,32,44–59]. This study specifically focuses on examining monometallic and bimetallic catalysts that have been exposed to the NO/ H_2 reaction. To the authors' knowledge this is the first work examining the interaction of NO with a synergistic Pt–Rh bimetallic catalyst for the NO/ H_2 reaction using in situ FTIR spectroscopy.

2. Experimental

2.1. Catalyst preparation

All catalysts were prepared using Norton SA 6375D γ - Al_2O_3 with a BET surface area of 258 m^2/g . The γ - Al_2O_3 was stabilized by

Table 1

Catalyst identification and metallic composition.

Notation	Pt wt%	Rh wt%	Pt/(Pt + Rh) mass ratio
Pt/ γ - Al_2O_3	0.83	0	N/A
Rh/ γ - Al_2O_3	0	0.89	N/A
95/5	0.83	0.04	0.95
90/10	0.83	0.09	0.90

calcining at 500 °C for 3 h. Platinum(IV) chloride (98% pure, Aldrich) and rhodium(III) chloride (38–41 weight percent Rh, Strem Chemicals) were used as precursors for the preparation of Pt- and Rh-containing catalysts. Monometallic catalysts were prepared via incipient wetness impregnation into stabilized γ - Al_2O_3 by an aqueous precursor solution that contained the necessary amount of metal precursor required to achieve the desired loading, typically 0.8–1.0% by weight. All catalysts were prepared using a ratio of precursor solution volume to support mass of 1.8 mL/g. Following impregnation, the catalysts were allowed to air dry for 12 h at room temperature. Pt catalysts were calcined at 500 °C for 3 h before being stored in a desiccator, while Rh catalysts underwent no further treatment and were stored in a desiccator immediately after drying. Bimetallic Pt–Rh catalysts were prepared by impregnating a calcined Pt catalyst with a $RhCl_3$ solution using the same procedure described above. Following impregnation, the bimetallic catalysts were dried in air at room temperature for 12 h and stored in a desiccator for later use. All catalysts were reduced in situ under flowing 0.7% H_2 in N_2 at 300 °C or 250 °C for 12 h prior to catalyst testing or FTIR studies, respectively. Table 1 lists the catalyst preparations and their sample notations.

2.2. Reactor studies

Fig. 1 shows the catalyst testing apparatus that was used to investigate the activity of the catalysts for the reduction of NO with H_2 . Certified gas mixtures (Gas Technology and Services, GTS), 0.7% NO in N_2 and 0.7% H_2 in N_2 , were blended to create the desired feed composition and flowrate using a bank of Gilmont Accucal rotameters. The pressure drop across the rotameters was controlled using a back pressure regulator (Tescom) which allowed each rotameter to be calibrated for consistent delivery of each component. A four-way valve was located before the reactor allowing the inlet or outlet gas composition to be measured. A

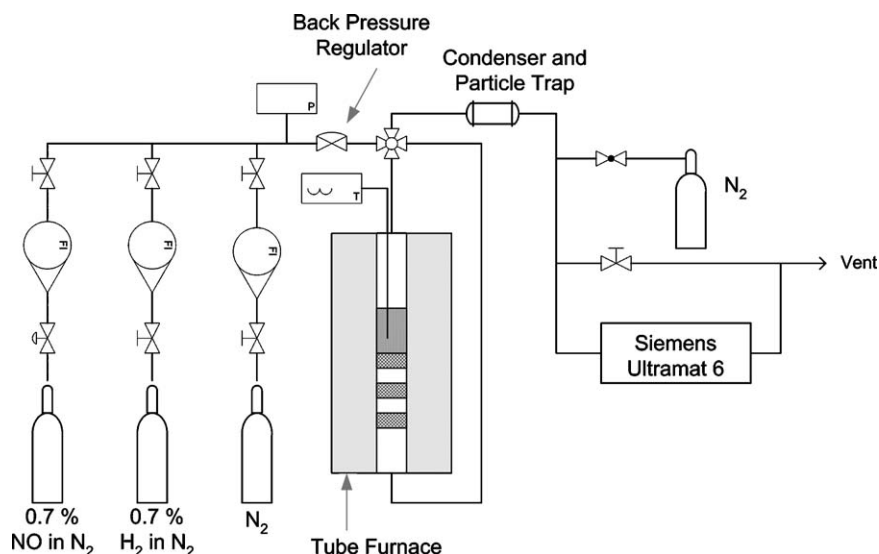


Fig. 1. Schematic of the continuous flow catalyst testing apparatus.

Siemens Ultramat 6 IR detector NO was used to detect NO. The reactor consisted of a quartz tube ($1.05\text{ cm} \times 1.30\text{ cm} \times 60.96\text{ cm}$, National Scientific) surrounded by a tube furnace with a machined ceramic insert. The temperature of the furnace was measured using an internal K-type thermocouple and was controlled using an Omega CN9000 temperature controller. The catalyst to be tested was supported in the center of the reactor tube on a glass wool plug. Two additional glass wool plugs were placed below the bed to capture any particulates that passed the first plug. Catalyst temperature was monitored using an axial K-type thermocouple inserted into the center of the catalyst bed.

The reduction of NO with H_2 was carried out over samples of catalyst with a mass of $\sim 2.2\text{ g}$ and a bed volume of 4.5 mL . In order to achieve a space velocity of $20\,000\text{ h}^{-1}$, the gas flowrate was set at 1500 mL/min , and the gases were blended to obtain a feed composition of 0.35% NO, 0.35% H_2 , and 99.3% N_2 . This feed composition and flowrate were selected based on the work of Lakis et al. [8] in an attempt to reproduce the synergy observed during their tests. Since the amount of NO exceeded the detection range of the Ultramat 6 analyzer ($0\text{--}1000\text{ ppm NO}$), the analyte was diluted with pre-purified N_2 (Airgas) in order to accurately measure the composition of NO. After loading a sample of catalyst into the reactor, it was reduced at $300\text{ }^\circ\text{C}$ for 12 h under 1500 mL/min of flowing 0.7% H_2 in N_2 . The catalyst sample was then allowed to cool to room temperature and was conditioned by equilibrating under reaction conditions at $250\text{ }^\circ\text{C}$ for 10 h . The NO/ H_2 reaction was then run over the catalyst approximately 3 times in order to measure the rate of reaction over a $35\text{ }^\circ\text{C}$ furnace temperature range, beginning at the temperature that NO conversion was initially observed. At least 5 steady state points were obtained over the applicable temperature range in $5\text{ }^\circ\text{C}$ furnace temperature increments. Between reaction studies, the catalyst was kept at room temperature under flowing N_2 .

2.3. Electron microscopy

A JEOL 2200 FS aberration-corrected scanning transmission electron microscope (STEM) was used to determine the size of the supported nanoparticles in the reacted bimetallic catalysts. Electron microscopy samples were prepared using a solvent-free method to disperse the catalyst on continuously carbon-coated 300 mesh Cu grids (Structure Probe, Inc.). Prior to dispersion, the catalyst was ground using a mortar and pestle for approximately 10 min . Dispersion was carried out by scooping the ground catalyst onto the carbon-coated side of the grid and then dumping the excess back into the mortar. This process was repeated 5–7 times to prepare a sample with suitable catalyst density. Annular Dark Field (ADF) images of several regions containing supported nanoparticles were acquired and particle size was measured digitally. Due to the differing particle shapes, particle sizes are reported as the average of the smallest and largest particle diameter. The measuring scheme along with the image resolution allowed the particle size to be conservatively reported to $\pm 0.1\text{ nm}$.

2.4. FTIR studies

Fig. 2 shows a schematic of the Fourier transform infrared (FTIR) system used for the study of NO adsorption on the previously tested catalysts. All spectra were obtained with a Thermo-Mattson Satellite FTIR instrument with 2 cm^{-1} resolution. The in situ cell was a Harrick Scientific demountable liquid cell equipped with an internal K-type thermocouple located close to the sample and two 100-W cartridge heaters. An Omega CN9000A temperature controller was used in conjunction with the internal thermocouple and cartridge heaters to control the cell temperature. The operating range for the in situ cell was from room temperature

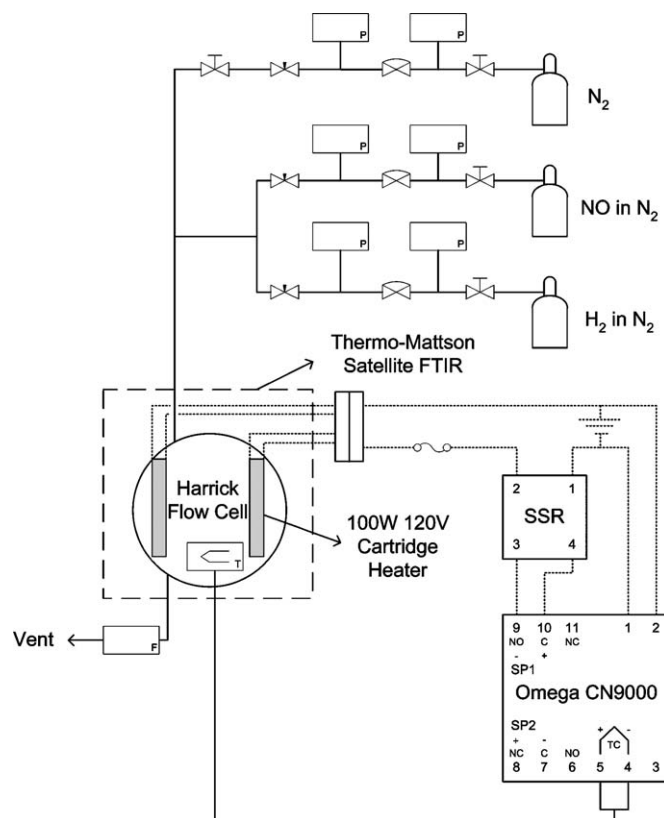


Fig. 2. Schematic of the in situ FTIR system with a temperature-controlled flow reaction cell.

up to $250\text{ }^\circ\text{C}$. The cell was designed such that a 13-mm diameter catalyst wafer could be placed between two 19 mm in diameter and 2 mm thick NaCl windows. A screw cap assembly and Kalrez o-rings were used to seal the cell. Catalyst wafers with mass $\sim 40\text{ mg}$ were prepared using a 13 mm die (International Crystal Laboratories) and a laboratory press (Carver) employing a force of 1.5 metric tons and a pressing time of 30 s . A set of three gas cylinders containing 0.7% NO in N_2 (certified, GTS), 0.7% H_2 in N_2 (certified, GTS), and N_2 (pre-purified, Airgas) were used to supply the gaseous feed for the FTIR cell. Needle valves were used to control the flowrate through the cell, and a bubble flow meter located after the cell was used to determine flowrate.

To conduct the NO or NO + H_2 interaction study, a catalyst wafer was placed in the in situ cell, and the sample was reduced at $250\text{ }^\circ\text{C}$ for 12 h under 0.7% H_2 in N_2 (certified, GTS) flowing at 30 mL/min . The sample was allowed to cool to the desired temperature ($100\text{ }^\circ\text{C}$, $150\text{ }^\circ\text{C}$, $200\text{ }^\circ\text{C}$, or $250\text{ }^\circ\text{C}$) under N_2 (pre-purified, Airgas) flowing at 12 mL/min . Following equilibration at the new temperature and N_2 atmosphere (a minimum of 2 h), a background spectrum was taken. For the interaction with NO, 0.7% NO in N_2 gas mixture (certified, GTS) was passed through the cell at 12 mL/min and spectra were taken in defined intervals for 1 h . For NO + H_2 interaction studies the catalyst was exposed to 12 mL/min of a $1:1$ mixture of 0.7% H_2 in N_2 (certified, GTS) and 0.7% NO in N_2 (certified, GTS) resulting in a feed composition of 0.35% NO, 0.35% H_2 , and 99.7% N_2 then spectra were taken in defined intervals for 1 h . If multiple tests were performed on a given sample, it was stored under flowing N_2 at 12 mL/min and was reduced at $250\text{ }^\circ\text{C}$ with 30 mL/min of flowing 0.7% H_2 in N_2 for 2.5 h prior to each test. Following interaction with NO + H_2 , $95/5$ was exposed to 12 mL/min of 0.7% H_2 in N_2 (certified, GTS) for 30 min then re-exposed to 12 mL/min of 0.35% NO, 0.35% H_2 , and 99.7% N_2 . Spectra were collected at 2 min intervals during these additional treatments.

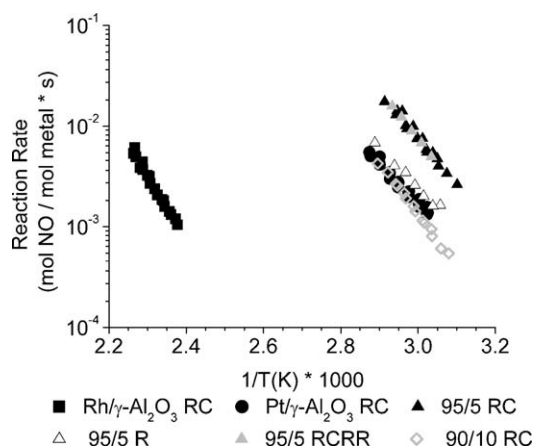


Fig. 3. Arrhenius plot of reaction rate (mmol NO/mol metal*s) vs. $1000/T$ for the reduction of NO with H_2 using a feed composition of 3500 ppm NO, 3500 ppm H_2 , and 99.7% N_2 with a space velocity of 20 000 h^{-1} . The sequence of alphanumeric characters following the catalyst identification corresponds to the thermal treatments other than activity testing that the catalyst received once placed in the reactor where R = reduction at 300 °C for 12 h and C = conditioning by equilibrating under reaction conditions at 250 °C for 12 h. For example, the notation 90/10 RC indicates that 90/10 was reduced for 12 h at 300 °C then exposed to reaction conditions at 250 °C for 12 h prior to activity testing. In the text all catalysts have undergone the RC thermal treatment unless otherwise noted.

3. Results

3.1. Catalyst testing

An Arrhenius plot using reaction rate for the y-axis was prepared to compare the relative activity of the catalysts (Fig. 3). Increased activity is indicated for rates towards the upper right-hand corner of the plot. The following order of relative activity can be inferred for the catalysts tested in this study: 95/5 > Pt/ γ - Al_2O_3 \approx 90/10 \gg Rh/ γ - Al_2O_3 . This observed order of relative activity is expected because it is same order observed by Lakis et al. for similar catalysts [8], excluding 90/10 since a catalyst of

this composition was not examined in that study. The maximum activity of 95/5, a five-fold increase over Pt/ γ - Al_2O_3 , was observed after conditioning the catalyst by equilibrating under reaction conditions for 10 h at 250 °C. Following reduction and prior to conditioning, 95/5 had an activity similar to Pt/ γ - Al_2O_3 . The activity of reduced, conditioned 95/5 was unaffected by a 24 h reduction at 300 °C. The reaction also was run over a sample of the support material only, and it was found to be inactive for this reaction over the temperature range used for catalyst testing.

3.2. Bimetallic catalyst particle-size measurements

To determine whether a difference in particle size could account for the increase in activity of 95/5 compared to 90/10, electron microscopy was used to acquire particle-size distributions of 95/5 and 90/10 (Fig. 4). The mean particle sizes of 95/5 and 90/10 were found to be $2.05 \text{ nm} \pm 0.07 \text{ nm}$ and $1.96 \pm 0.05 \text{ nm}$, respectively, where the error represents the 95% confidence interval on the mean. Visual examination of the particle-size distributions presented in Fig. 4 indicates that the particle-size distribution of 90/10 is wider than that of 95/5, which is also evident statistically in the standard deviations of the particle populations ($\sigma_{95/5} = 0.52 \text{ nm}$ and $\sigma_{90/10} = 0.66 \text{ nm}$). Although the particle-size distribution of 90/10 is wider than that of 95/5, it has a smaller confidence interval on the mean due a larger sample size ($n_{95/5} = 200$ and $n_{90/10} = 576$). Performing a two-sample *t*-test on the particle-size distributions of 95/5 and 90/10 shows with 99% confidence that the difference between the mean particle size of 95/5 and 90/10 is zero.

3.3. FTIR studies

3.3.1. Support-bound species

Exposing γ - Al_2O_3 , Pt/ γ - Al_2O_3 , Rh/ γ - Al_2O_3 , 95/5, and 90/10 to an NO-containing atmosphere resulted in several peaks being observed between 1200 cm^{-1} and 1700 cm^{-1} that can be assigned to a variety of nitrates and nitrites on the alumina surface (Table 2). Since the focus of this study is on the surface of the bimetallic nanoparticles, only an example of the spectral region containing

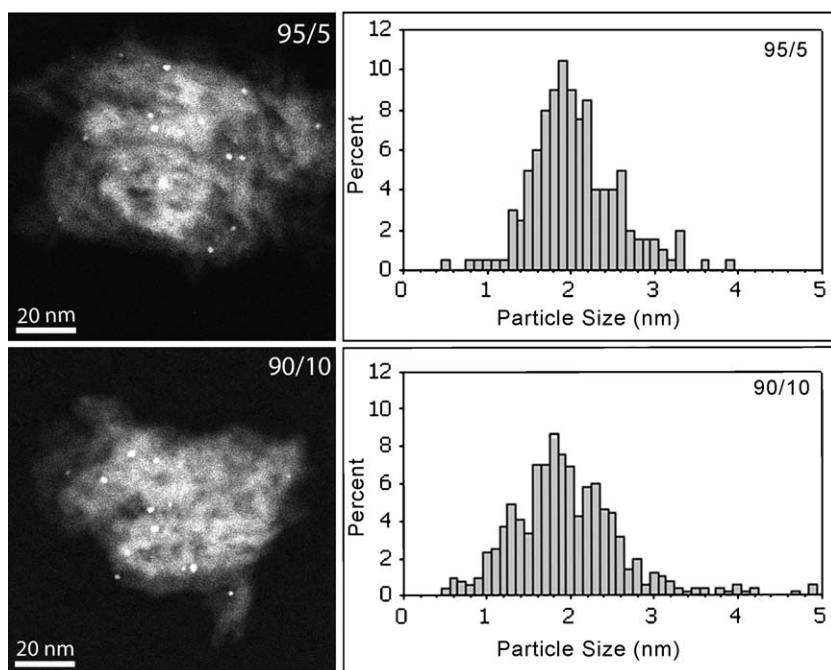


Fig. 4. Particle-size distributions and example images of 95/5 (top) and 90/10 (bottom). The particle-size distribution histograms are reported using percent of total as the y-axis due to the difference in sample size. For 95/5 the sample size is 200 particles, and for 90/10 the sample size is 576 particles.

Table 2

Potential and observed support- and metal-bound IR active species.

Peak #	Species	Observed position ^a	Structure ^b	Reference
1	Bridged bidentate nitrite	a: 1230 cm ⁻¹ b: 1310 cm ⁻¹		[32,55,57,59]
2	Monodentate nitrite	1440 cm ⁻¹	Al-O-N-O	[57,58]
3	<i>n</i> -Coordinated nitrite	1530 cm ⁻¹		[32,56,57]
4	Monodentate nitrate	Not observed		[58]
5	Chelating bidentate nitrate	1585 cm ⁻¹		[32,55–57]
6	Bridged bidentate nitrate	1650 cm ⁻¹		[32,50,54–59]
7	Linear NO on Pt	100 °C: 1750 cm ⁻¹ 150–250 °C: 1760 cm ⁻¹	Pt ⁰ -NO	[32,36,50,60]
8	Bent NO on Pt	Not observed	Pt ⁰ -NO	[32,50]
9	Anionic NO on Rh	(a) Low: 1695 cm ⁻¹ (b) High: 1770 cm ⁻¹	Rh ⁰ -NO ^{δ-}	[45,47,61]
10	Neutral NO on Rh	1800 cm ⁻¹	Rh ⁰ -NO	[47]
11	Rh nitrosyl (cationic NO on Rh)	1905 cm ⁻¹	Rh ⁺ -NO ^{δ+} Rh ^{δ+} -NO ^{δ+}	[18,44,45,47,51,61,69]
12	Rh dinitrosyl	Not observed	Rh (NO ₂)	[45,50]

See Section 3.3.2 for more information.

^a Peak assignments presented in this table are those observed in this study and were chosen based on evidence included in the cited references.^b Structure for each species is based on information obtained from references associated with that species.^c Under NO + H₂ at 200 °C and 250 °C the linear NO on Pt peak appears as a doublet centered at this location.

the alumina-bound nitrates and nitrites observed is presented (Fig. 5). While differences in peak magnitude were observed with changes in the catalyst and temperature, evidence of these peaks was present in all the samples. The peaks observed at 1230 cm⁻¹

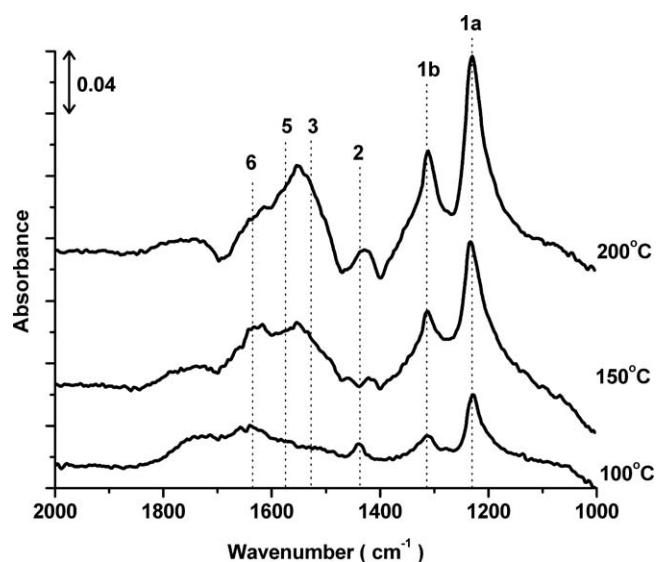


Fig. 5. Infrared spectra obtained during exposure of 95/5 to 0.7% NO in N₂ with 95/5 at 100 °C, 150 °C, and 200 °C. For clarity, only peaks associated with alumina-bound nitrates and nitrites are identified (Table 2); refer to Fig. 6 for the identification of NO-metal species.

and 1310 cm⁻¹, labeled 1a and 1b, are assigned to a bridged bidentate nitrite species [32,55,57,59]. Peak 2, observed at 1440 cm⁻¹, is assigned to a monodentate nitrite species [57,58]. The region between 1500 cm⁻¹ and 1600 cm⁻¹ contains peaks, numbers 3 and 5, which are assigned to *N*-coordinated nitrite (1530 cm⁻¹) [32,56,57] and chelating bidentate nitrate (1585 cm⁻¹) [32,55–57]. There is a possibility that monodentate nitrate species, peak 4 in Table 2, could also exist in this range; however, our experimental conditions were such that this species should not form [58]. The broad peak, labeled 6, at 1650 cm⁻¹ is assigned to bridged bidentate nitrate [32,50,54–59].

3.3.2. Pt/γ-Al₂O₃

The interaction of 0.7% NO in N₂ with Pt/γ-Al₂O₃ was monitored with FTIR spectroscopy at 100 °C, 150 °C, and 200 °C (Fig. 6). For the 100 °C and 150 °C tests, the peak assigned to linearly adsorbed NO on Pt (peak 7) is clearly visible with the peak center occurring at 1750 cm⁻¹ and 1760 cm⁻¹, respectively. The difference in the central position of this peak can be attributed to the adsorption of NO on different types of Pt sites [32,36,60]. For the test conducted at 200 °C, the peak associated with linear NO on Pt has significantly decreased in magnitude, but is still centered at 1760 cm⁻¹. Bent NO species adsorbed on Pt, peak 8 in Table 2, are generally observed between 1650 cm⁻¹ and 1400 cm⁻¹ [32]; however, peaks associated with surface nitrates and nitrites are observed in this region, so any peaks resulting from bent NO on Pt will be difficult to detect unless they have significant magnitude. No significant peaks were found that could be definitively associated with bent NO on Pt for the Pt/γ-Al₂O₃ catalyst.

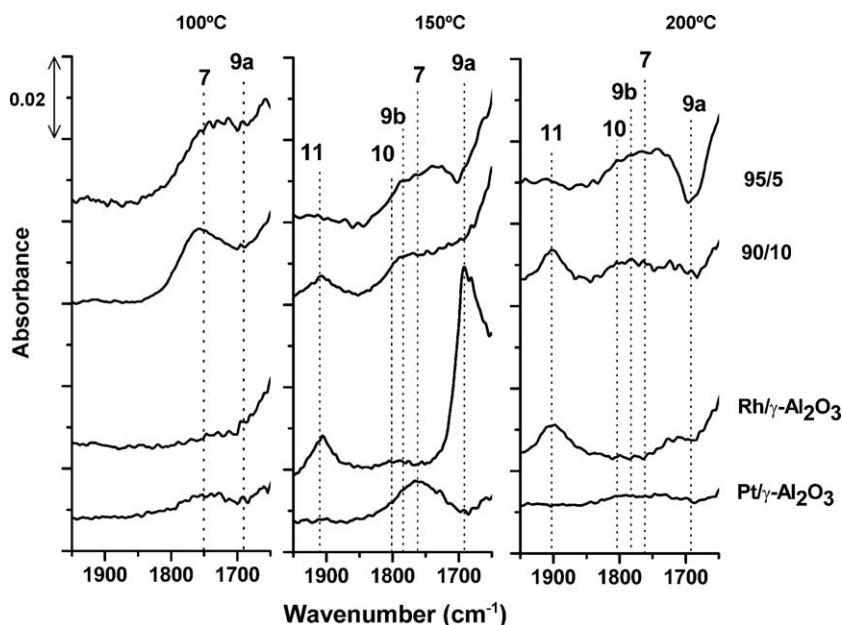


Fig. 6. Comparison of NO-metal region from the FTIR spectra obtained from exposing Pt/ γ -Al₂O₃, Rh/ γ -Al₂O₃, 95/5, and 90/10 to 0.7% NO in N₂ at 100 °C, 150 °C, and 200 °C for 60 min. Refer to Table 2 for peak assignments.

The presence of a peak associated with linear NO on Pt was also observed during the interaction of NO + H₂ with Pt/ γ -Al₂O₃ at 100 °C, 150 °C, 200 °C, and 250 °C (Fig. 7). At 100 °C and 150 °C the linear NO-on-Pt peak, labeled 7, appears as a broad peak centered at 1750 cm⁻¹ and 1760 cm⁻¹, respectively. At 200 °C and 250 °C the peak associated with linear NO on Pt appears as a doublet centered at 1760 cm⁻¹. The difference in shape and central position of this peak is attributed to NO binding to different types of Pt sites on the nanoparticle surface [32]. Unlike the interaction of NO with Pt/ γ -Al₂O₃, under reaction conditions, the maximum magnitude of the linear NO-on-Pt peak was observed at 100 °C and a trend of decreasing magnitude with increasing temperature was observed.

3.3.3. Rh/ γ -Al₂O₃

The interaction of 0.7% NO in N₂ with Rh/ γ -Al₂O₃ was monitored with FTIR spectroscopy at 100 °C, 150 °C, and 200 °C (Fig. 6). At 100 °C no distinct peaks associated with the NO adsorbed on Rh are present. The spectra at 150 °C has four peaks associated with the adsorption of NO on Rh including 1695 cm⁻¹ (labeled 9a), 1770 cm⁻¹ (labeled 9b), 1800 cm⁻¹ (labeled 10), and 1905 cm⁻¹ (labeled 11). Peaks 9a and 9b are assigned to low- and high-frequency anionic NO on Rh, respectively [45,47,51], and peak 10 is assigned to neutral NO on Rh [47]. Peak 11 is assigned to cationic NO on Rh (the Rh nitrosyl species), which results from NO adsorbed on partially or fully oxidized Rh [18,44,45,47,51,61]. It should be noted that peaks 9b and 10 are convolved and have

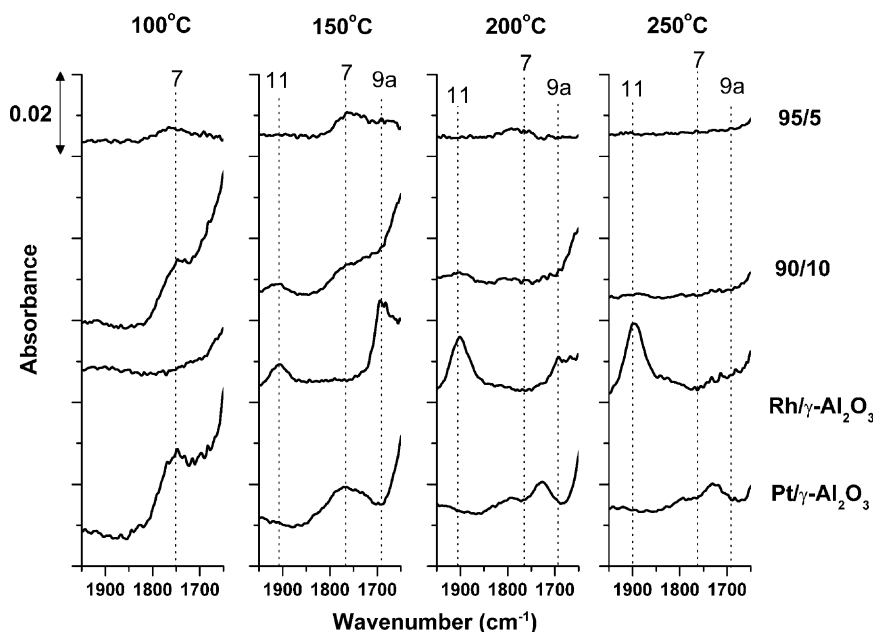


Fig. 7. Comparison of NO-metal region from the FTIR spectra obtained from exposing Pt/ γ -Al₂O₃, Rh/ γ -Al₂O₃, 95/5, and 90/10 to 0.35% NO, 0.35% H₂, and 99.7% N₂ at 100 °C, 150 °C, 200 °C, and 250 °C for 60 min. Refer to Table 2 for peak assignments.

significantly less magnitude than peaks 9a and 11. In the test conducted at 200 °C the peaks at 1770 cm^{-1} , labeled 9b, and 1800 cm^{-1} , labeled 10, are no longer visible, the peak at 1695 cm^{-1} , labeled 9a, has significantly decreased in magnitude, and peak 11 at 1905 cm^{-1} is still significant. Although gem-dinitrosyl species have previously been observed when NO interacts with Rh-containing catalysts [46,48,51,61], they were not observed in this study.

Similar trends in the observed NO-Rh species were observed for the interaction of NO + H₂ with Rh/ γ -Al₂O₃ (Fig. 7). The primary difference between the spectra collected under reaction conditions and during exposure to NO in N₂ is the difference in the magnitude of peaks associated with the NO-Rh species. While the Rh nitrosyl peak, labeled 11, has a similar magnitude at 150 °C and 200 °C during the interaction NO with Rh/ γ -Al₂O₃, under reaction conditions this peak shows a clear trend of increasing magnitude from 150 °C to 250 °C. Another difference in the spectra is that under reaction conditions at 150 °C there is no evidence of peaks associated with high-frequency anionic NO on Rh, peak 9b, and neutral NO on Rh, peak 10, while traces of these peaks were visible at this temperature during the interaction of NO. Similar trends in the magnitude of the low-frequency anionic NO on Rh peak were observed under reaction conditions as were observed during NO interaction.

3.3.4. 90/10 Pt-Rh/ γ -Al₂O₃

The interaction of 0.7% NO in N₂ with 90/10 was monitored with FTIR spectroscopy at 100 °C, 150 °C, and 200 °C (Fig. 6). At 100 °C a broad peak with a maximum at 1760 cm^{-1} was observed. This peak is assigned to linear NO on Pt labeled 7. Traces of low-frequency anionic NO on Rh may be present at 1695 cm^{-1} , labeled 9a; however, this peak cannot be distinguished because the low-wavenumber side of the broad peak at 1760 cm^{-1} is convolved with the bridging bidentate nitrate peak at 1650 cm^{-1} . At 150 °C a broad peak centered at 1760 cm^{-1} is visible, but this peak does not have a maximum at its center as was observed at 100 °C. This difference in shape occurs due to decreased magnitude in the region of peak 7 and increased magnitude in the region of peak 9a.

A distinct peak at 1905 cm^{-1} , labeled 11, which corresponds to cationic NO on oxidized Rh, is also visible at 150 °C. At 200 °C peak 11 has increased in magnitude, and the magnitude of the broad peak centered at 1760 cm^{-1} has decreased. This peak has a similar width to the peak associated with linear NO on Pt in Pt/ γ -Al₂O₃ at 200 °C; however, it has increased magnitude especially in the regions of neutral and high-frequency anionic NO on Rh, labeled 10 and 9b. Although there is an increase in magnitude in the region of peaks 9b and 10, the presence of these peaks cannot be verified because they are convolved with peak 7.

The spectra obtained from 90/10 under reaction conditions show similar features to those obtained during the interaction of NO with several minor differences (Fig. 7). At 150 °C and 200 °C, the broad peak centered at 1760 cm^{-1} and peak 11 at 1905 cm^{-1} have lower magnitude than was observed during the NO interaction studies. At 100 °C, the peak associated with linear NO on Pt has a maximum at 1750 cm^{-1} , 10 cm^{-1} lower than was observed during the NO interaction studies. It is possible that the increased magnitude at the low-wavenumber side of this peak is partially due to the presence of low-frequency anionic NO on Rh; however, it cannot be confirmed because it is convolved with the bridging bidentate nitrate peak. Peaks associated with NO-metal species were not observed at 250 °C.

3.3.5. 95/5 Pt-Rh/ γ -Al₂O₃

The interaction of 0.7% NO in N₂ with 95/5 was monitored with FTIR spectroscopy at 100 °C, 150 °C, and 200 °C (Fig. 6). For the 100 °C test, a broad peak centered at 1740 cm^{-1} was observed. The majority of the magnitude of this peak is associated with linear NO on Pt, labeled 7. The low-frequency edge of the broad peak centered at 1740 cm^{-1} potentially contains a peak at 1695 cm^{-1} representative of low-frequency anionic NO on Rh, labeled 9a; however, it is not distinctly visible because it is also convolved with peak 6, at 1650 cm^{-1} . At 150 °C, a broad peak centered 1750 cm^{-1} is visible; this peak is primarily composed of linear NO on Pt, labeled 7. It is possible that some of the magnitude of this peak is from anionic and/or neutral NO on Rh (peaks 9a, 9b, and 10). At 200 °C, a broad peak centered at 1760 cm^{-1} is observed that

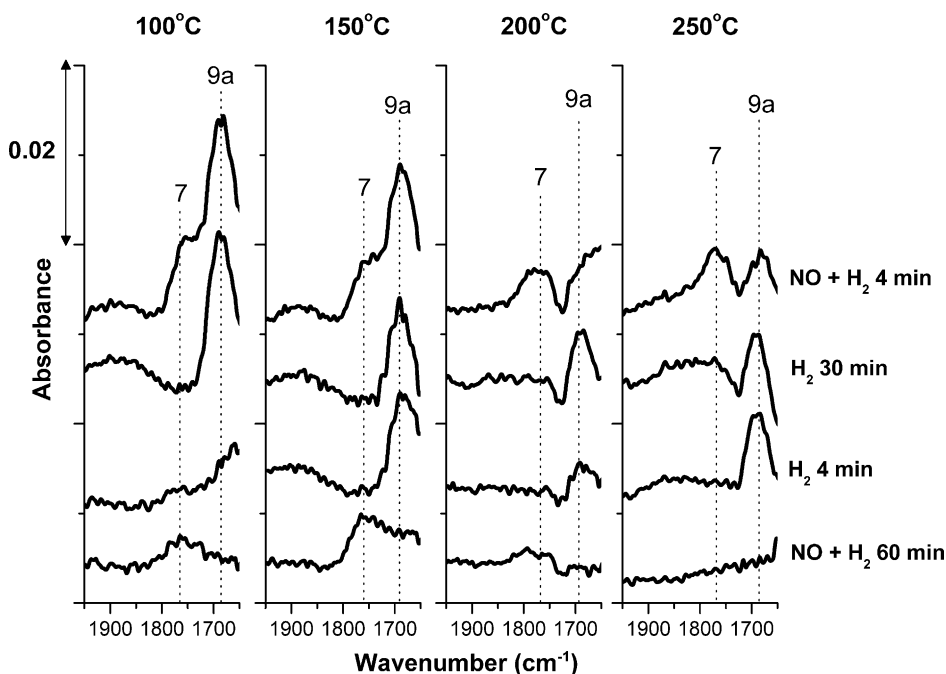


Fig. 8. FTIR spectra obtained from 95/5 following exposure to 0.35% NO in N₂ and 0.35% H₂ in N₂ for 60 min followed by 0.7% H₂ in N₂ for 30 min and re-exposure to NO + H₂. Refer to Table 2 for peak assignments.

is primarily associated with NO linearly adsorbed on Pt, labeled 7. It is possible some of the magnitude in the high-wavenumber edge of this peak results from high-frequency NO adsorbed on Rh (labeled 9b) and neutral NO adsorbed on Rh (labeled 10). A distinct difference in the NO-metal adsorption region of the spectra in the tests at 100 °C and 150 °C compared to the test at 200 °C is the absence of intensity in the region of peak 9a in the 200 °C test. The presence of peaks 9b and 10 cannot be confirmed at all temperatures because they are convolved with the linear NO on Pt peak, labeled 7.

FTIR spectra were also obtained from 95/5 under reaction conditions at 100 °C, 150 °C, 200 °C, and 250 °C (Fig. 7). At 100 °C, 150 °C, and 200 °C a peak associated with linear NO on Pt was observed at 1760 cm⁻¹, and at each of these temperatures this peak has significantly less magnitude than the linear NO-on-Pt peaks observed during the NO interaction studies. No significant evidence of low-frequency anionic NO was observed at 100 °C and 200 °C; however, a small peak is visible at 1695 cm⁻¹, labeled 9a, for the test at 150 °C. At 250 °C no evidence of peaks associated with NO-metal species were observed.

The surface of 95/5 was further probed following exposure to reaction conditions for 60 min by exposing the catalyst to 0.7% H₂ in N₂ for 30 min then re-exposing it to reaction conditions (Fig. 8). Following the initial 60 min exposure to reaction conditions at 100 °C, 150 °C, 200 °C, and 250 °C the NO-metal region of the spectra shows features as described in the previous paragraph. Following 4 min of exposure to 0.7% H₂ in N₂, any visible peaks associated with linear NO adsorbed on Pt disappear, and a peak associated with low-frequency anionic NO on Rh appears at 1695 cm⁻¹, labeled 9a. The magnitude of this peak varied with temperature and does not have a clear trend with the largest magnitudes being observed at 150 °C and 250 °C. Following 30 min of interaction with 0.7% H₂ in N₂, peak 9a is still visible at all four temperatures and has the following relative order of intensity: 100 °C > 150 °C > 200 °C ≈ 250 °C. After 4 min of re-exposure to reaction conditions, peak 9a remains and a peak associated with linear NO on Pt, labeled 7, appears at all four temperatures.

4. Discussion

4.1. Probing Pt and Rh with NO and NO + H₂

Since NO does not readily adsorb on γ -Al₂O₃ [62], it primarily interacts with the catalysts through molecular or dissociative adsorption on the supported metals, which resulting in the formation of adsorbed NO, N, and O species. Adsorbed O can also form through the surface reaction of adsorbed N and adsorbed NO [63]. For the FTIR studies under reaction conditions, H₂ is also present in the feed which results in the formation of other surface species including adsorbed H and H-containing intermediates [63]. Of the potential metal-adsorbed surface species, molecularly adsorbed NO is the only one that is readily observed with FTIR spectroscopy. Since molecularly adsorbed NO is not the only species present on the metal surface under our experimental conditions, peak intensity associated with NO-metal bonds cannot be used to quantify the amount of exposed metal on the surface of the supported bimetallic nanoparticles. Observation of these peaks, however, does confirm the presence of a particular metal species on the surface of the supported nanoparticles.

A distinct mechanistic difference exists during NO interaction and under reaction conditions due to the fate of the adsorbed oxygen species. The recombination of adsorbed O to form gaseous O₂ is not favored at temperatures below 700 °C on platinum group metal surfaces [4,62], so during the NO interaction studies possible mechanisms for the removal of adsorbed O include spillover onto the support and combination with adsorbed or gas-phase NO to

form NO₂. Under reaction conditions, however, the presence of hydrogen allows adsorbed O to be removed through water formation, thus increasing the number of sites available for molecular or dissociative NO adsorption. Since dissociative adsorption of NO results in species that cannot be viewed with FTIR spectroscopy, conditions or surfaces which favor the dissociative NO adsorption should result in decreased intensity for peaks associated with NO-metal vibrations.

The prepared catalysts were examined with NO in N₂ and NO + H₂ in N₂ because it was not known which interactions would produce the most favorable surface conditions for observing both Pt and Rh. Levy et al. previously developed a method for quantifying the surface composition of Pt and Rh on Pt-Rh/Al₂O₃ catalyst using the irreversible adsorption of CO and NO [51]. That method produced reasonable results compared to traditional H₂ chemisorption for the overall metal surface area and showed Rh surface enrichment in all of the examined samples. A similar procedure was not employed here because it involves using a probe (CO), which is not present under our reaction conditions, as well as pressures much lower than those used in this study (~0.02 atm). Working under different conditions and using probes that are not present in our reaction system is undesirable because it could alter the surface composition of the supported alloy nanoparticles.

Understanding the interaction of NO in N₂ and NO + H₂ in N₂ with the monometallic catalysts is important for establishing a baseline for the potential NO-metal peaks that could be observed on the bimetallic catalysts. Linear NO on Pt was generally observed as a broad peak centered at 1760 cm⁻¹ (peak 7 in Figs. 6 and 7). At all temperatures except 150 °C, more intensity from peaks associated with linear NO on Pt species were observed under reaction conditions than during NO adsorption. The decreased intensity for the NO interaction studies is likely due to an increased fraction of adsorbed N and/or O on the catalyst surface. Differences in the shape, width, and position of the linear NO on Pt peak are the result of NO adsorption on different types of Pt sites [32]. The presence of NO adsorbed on Rh was primarily observed as low-frequency anionic NO on Rh at 1695 cm⁻¹, labeled 9a, and cationic NO on oxidized Rh, labeled 11 (Figs. 6 and 7). The absence of any NO-Rh peaks at 100 °C is attributed to significantly decreased NO adsorption. The decreased intensity of the low-frequency anionic NO on Rh peak at 200 °C is attributed to increased amount of dissociative NO adsorption compared to molecular NO adsorption. For the NO interaction study, the Rh nitrosyl peak shows similar magnitude at 150 °C and 200 °C, while under reaction conditions a trend of increasing magnitude is observed from 150 °C to 250 °C. The trend of increasing magnitude as a function of increasing temperature observed during reaction conditions could be a result of the presence of more oxidized Rh on the catalyst surface due to increased oxidative disruption of NO. It is also possible that this trend occurs because hydrogen removes some of the adsorbed oxygen resulting in increased molecular adsorption of NO.

4.2. Confirming the presence of surface Pt and Rh on 90/10 and 95/5

The presence of Pt and Rh on the surface of 90/10 and 95/5 is confirmed through the observation of peaks associated with NO-metal species in the FTIR spectra. The absence of these peaks, however, does not prove that these metals are not present on the surface of the alloy nanoparticles. The presence of Pt and Rh on the surface of 90/10 under reaction conditions and during NO adsorption has been confirmed at 150 °C and 200 °C through the observation of the linear NO-on-Pt peak and the Rh nitrosyl peak (peaks 7 and 11 in Figs. 6 and 7). At 100 °C the presence of Rh cannot be confirmed, but this is not surprising because evidence of NO-Rh species were not observed on Rh/ γ -Al₂O₃ at 100 °C.

Identification of Rh through the observation of the Rh nitrosyl peak indicates that the Rh is oxidized. Since Pt is known to hinder the oxidation of Rh [11], it is likely that some metallic Rh is also present on the surface of the nanoparticles in 90/10, although it was not directly observed.

Since the Rh nitrosyl peak was not observed on 95/5 during the interaction of NO + N₂ and under reaction conditions, the presence of Rh on the surface of 95/5 could not be confirmed because peaks associated with neutral and anionic NO on Rh are convolved with the linear NO-on-Pt peak. The linear NO-on-Pt peak was, however, clearly visible under reaction conditions confirming the presence of metallic Pt on the surface of 95/5. Since previous researchers have identified NO- and/or O₂-induced Rh surface segregation in Pt-Rh alloys using ultra high vacuum techniques [14,22–31], surface-segregated Rh was expected to be present on the surface of the Pt-Rh alloy nanoparticles of 95/5. Since the catalysts were equilibrated to N₂ prior to the FTIR studies, it was decided that introducing a reducing agent to remove some of the adsorbed species then reintroducing NO + H₂ would increase the probability of observing NO adsorbed on Rh. As described in Section 3.3.5, this treatment procedure resulted in the observation of linear NO on Pt and low-frequency anionic NO on Rh at 100 °C, 150 °C, 200 °C, and 250 °C, confirming the presence of metallic Pt and Rh on the surface of 95/5 under reaction conditions.

4.3. The synergistic performance of 95/5 and the non-synergistic performance of 90/10

The reduction of NO with H₂ over supported metal catalysts results in the production of N₂, N₂O, NH₃, and H₂O. The following mechanistic steps are typically associated with the production of N₂ on noble metal surfaces, where S denotes a surface site [63–68]:



Recently it has also been suggested that N₂ production is also possible through adsorbed NH_x species [67]. The production of N₂O can occur through the following steps [63–68]:



NH₃ production occurs through the sequential combination of adsorbed H and adsorbed N through NH_x intermediates, and water is produced through the combination of adsorbed O with 2 adsorbed H [63,64,66–68].

Analysis of the mechanistic steps presented above for the production of N₂ and N₂O shows that N₂O production requires the presence of adsorbed NO, while N₂ production can proceed in the presence or absence of the adsorbed NO species. Thus, minimizing linear NO adsorption under reaction conditions should decrease the production of N₂O and aid the production of N₂ through recombination of adsorbed N, Eq. (1). Comparing the spectra obtained under reaction conditions (Fig. 7), less molecularly adsorbed NO is observed on 95/5 at each temperature than the other monometallic catalysts except Rh/γ-Al₂O₃ at 100 °C. This difference with Rh/γ-Al₂O₃ is not significant because at this temperature 95/5 is operating at nearly complete conversion, while Rh/γ-Al₂O₃ is barely active. At 250 °C molecularly adsorbed NO was not observed on 95/5, while it was observed on the monometallic catalysts at this temperature. This suggests that 95/5 should be more selective than the monometallic catalysts, especially at elevated temperature. Although selectivity data was not collected on this series of catalysts, Lakis et al. found that a Pt(95%)-Rh(5%)/γ-Al₂O₃

catalyst similar to the one examined in this study had comparable selectivity to a Pt/γ-Al₂O₃ and Rh/γ-Al₂O₃ catalyst up to 210 °C. At 275 °C the ratio of N₂O production to N₂ production approached 100:1 while it was approximately 2.5:1 for the monometallic catalysts [8]. Coupling the selectivity data collected by Lakis et al. with the FTIR observations from this study, it can be inferred that the absence of molecularly adsorbed NO leads to increased selectivity towards N₂.

Since molecularly adsorbed NO was not observed on either bimetallic catalyst at 250 °C under reaction conditions, both bimetallic surfaces dissociate NO and remove the resulting adsorbed oxygen more effectively than the monometallic catalysts under these conditions. Although similar overall magnitude is observed for molecularly adsorbed NO species on 90/10 and 95/5 at 200 °C, the observed peaks differ in that on 95/5 only molecularly adsorbed NO on Pt was observed whereas on 90/10 both the molecularly adsorbed NO on Pt and Rh nitrosyl peaks were observed. Observation of the Rh nitrosyl peak indicates that the Rh is either partially or fully oxidized [47,69]. Although NO adsorbed on Rh⁰ was not directly observed it is possible that this species also exists on the surface.

To explain whether the Rh observed in 90/10 via the Rh nitrosyl peak is fully or partially oxidized, it is necessary to define the morphology of the supported metal nanoparticles in reference to previous research as well as the observations in this study. The preparation procedure and thermal treatments applied to both 95/5 and 90/10 have previously been shown to result in the formation of Pt-Rh alloy nanoparticles [7,8,14–16], so it can safely be assumed that Pt-Rh alloying has occurred in 95/5 and 90/10. Based on a comparison of the bulk composition of 95/5 to the low-temperature miscibility gap in the Pt-Rh phase diagram and the AEM study performed by Lakis et al. on a similar catalyst [7], a single phase of Pt-rich, Pt-Rh alloy nanoparticles should exist in 95/5. Since the composition of 90/10 within the low-temperature miscibility gap in the Pt-Rh phase diagram, it is possible that the Pt-Rh alloy nanoparticles could phase separate into a Pt-rich phase and Rh-rich phase. If phase separation occurs, the Rh-rich phase would only account for 6% of the nanoparticles present in the system and the Pt-rich phase would have a similar composition, and thus activity, as 95/5. This calculation was performed based on the low-temperature miscibility gap proposed by Lakis et al. [7] assuming phase separation occurred during reduction at 300 °C. Considering the proposed level of segregation (94% Pt-rich particles and 6% Rh-rich particles) and that the created Rh-rich phase is inactive (the worst possible scenario), phase-separated 90/10 would have an estimated activity that is 94% of the activity observed for 95/5. This predicted activity is 425% higher than the observed activity of 90/10, which suggests phase separation alone cannot account for the difference in activity between 95/5 and 90/10. Thus, it is expected that less phase separation than was predicted occurred in 90/10 resulting in the Pt-rich particles of 90/10 having an increased Rh composition compared to the Pt-rich particles of 95/5. A difference in particle size does not contribute to the lower activity of 90/10 compared to 95/5 because 95/5 and 90/10 have similar particle-size distributions and a statistically significant difference in the mean particle size was not observed at 99% confidence (Fig. 4).

Since it can be safely assumed that most metal particles on 90/10 are Pt-rich, the oxidized Rh observed on this catalyst is believed to be present on the surface of the Pt-Rh alloy nanoparticles. A distinct difference in the surface morphology of the Pt-rich phase of 95/5 and 90/10 must exist because oxidized Rh was not observed on 95/5. Rh can take on a partially oxidized character, Rh^{δ+}, through the presence of adsorbed O withdrawing electron density from Rh [69]. The subsequent adsorption of NO on Rh^{δ+} results in transfer of electron density from the adsorbed NO

species to $\text{Rh}^{\delta+}$ resulting in NO also taking on a partial positive charge [69]. It is unlikely that this would occur on a single Rh atom surrounded by Pt, rather it is more likely that this would occur on a group of Rh atoms with adsorbed O and NO atoms. Thus, the proposed difference in surface morphology between 95/5 and 90/10 is the presence of clusters of Rh surrounded by Pt on the surface of 90/10, while the surface of 95/5 only has single atoms of Rh surrounded by Pt. This morphology is supported by the NO interaction studies, where increased adsorbed O is likely present, because partially oxidized Rh was observed on 90/10 through the Rh nitrosyl peak at 150 °C and 200 °C and it was not observed on 95/5 under the same conditions.

The proposed difference in morphology between the surface of 95/5 and 90/10 is attributed to an increased amount of Rh in the Pt-Rich particles of 90/10. A higher Rh composition in the alloy nanoparticles raises the probability of having an increased fraction of Rh segregated to the particle surface. The role of Rh in Pt-Rh bimetallic catalysts during the reduction of NO with H_2 is to provide a site for the adsorption and dissociation of NO, and the role of Pt is to provide a site for the dissociative adsorption of H_2 [8]. The primary role of adsorbed H is to remove adsorbed O that is produced by NO dissociation. Therefore, the presence of increased Rh on the surface of 90/10 results in a decreased number of Pt sites for H_2 adsorption slowing removal of adsorbed O. The presence of increased adsorbed O on Rh surfaces is known to hinder NO adsorption [69], which could also result in decreased activity. Additionally, the presence of adsorbed oxygen causes Rh to take a partially oxidized character [69], which favors the formation of the stable Rh nitrosyl species. Since the Rh nitrosyl species is less likely to dissociate than anionic NO on Rh [47], the presence of increased adsorbed oxygen also hinders NO dissociation. Thus, 90/10 is less active than 95/5 due to the presence of increased fraction of Rh on the catalyst surface. The synergistic performance of 95/5 is due to the presence of a favorable ratio of Pt to Rh sites on the surface of the alloy nanoparticles that allows complimentary amounts of dissociative H_2 adsorption and dissociative NO adsorption.

4.4. Stability and conditioning of 95/5

In the process of attempting to identify Pt and Rh on the surface of 95/5 an interesting result was obtained; exposing 95/5 to a reducing atmosphere following 60 min of exposure to reaction conditions resulted in all traces of the peak associated with the linear NO on Pt peak disappearing and a peak associated with low-frequency anionic NO on Rh appearing at all four temperatures (Fig. 8). Removing NO from the feed resulted in the rapid reaction of the linear NO-on-Pt species, as was expected; however, the appearance of a peak associated with low-frequency anionic NO on Rh at all four temperatures was unexpected, especially because it remained visible through the duration of the reducing treatment, 30 min. It is important to consider that, according to equilibrium surface segregation, Pt should segregate to the surface of Pt-Rh nanoparticles because it has a lower surface energy than Rh, 2.5 J/m² vs. 2.7 J/m² [19]. Since NO adsorbs more strongly on Rh than on Pt [40,41], it is capable of shifting the chemical equilibrium allowing the surface segregation of the higher surface-energy element, Rh [20].

The formation of low-frequency anionic NO on Rh under reducing conditions following exposure to reaction conditions provides insight into why the activity of conditioned 95/5 was unchanged by a 24 h reduction at 300 °C (Fig. 3). The formation of the low-frequency anionic NO on Rh during H_2 reducing treatments allows Rh to remain surface segregated while being exposed to an atmosphere that favors a Pt-rich surface. Since this reducing treatment was only monitored with FTIR spectroscopy for 30 min at each of the temperatures in this study, it is possible that

longer times or increased temperatures could cause this species to break down resulting in Pt surface segregation as was observed on Pt-Rh single crystals during reduction treatments [24–27]. Since the activity of 95/5 was unaffected by a 24 h reduction at 300 °C, it is expected that the surface composition and particle morphology was not significantly altered by this treatment.

Prior to conditioning, by equilibration under reaction conditions at 250 °C for 10 h, the activity of 95/5 was similar to that of Pt, which suggests that following the initial reduction treatment the surface of 95/5 was primarily covered with Pt as is predicted by equilibrium surface segregation. If this is the case, conditioning the catalyst induced Rh surface segregation in the supported alloy nanoparticles forming the active surface. Formation of the active surface is believed to be aided at the conditioning temperature by the increased rate of diffusion of atoms within the supported alloy nanoparticles which increases the possibility of Rh reaching the surface. Once Rh reaches the surface, adsorbed O or NO shifts the chemical equilibrium allowing Rh to remain surface segregated even though it has a higher surface energy than Pt.

5. Conclusions

Observations of metal-adsorbed NO species with in situ FTIR spectroscopy confirmed the presence of Pt and Rh on the surface of the alloy nanoparticles in the catalysts 95/5 and 90/10. The synergistic performance of 95/5 is attributed to a favorable number of Pt and Rh sites on the surface of the supported alloy nanoparticles that allow complimentary amounts of H_2 adsorption and NO dissociation, respectively. The non-synergistic performance of 90/10 is attributed to a decreased fraction of Pt on the surface of the supported nanoparticles compared to 95/5 resulting in decreased H_2 adsorption and an increased fraction of surface-segregated Rh that can take on a partially oxidized character and inhibit NO adsorption and dissociation. The maximum activity of 95/5 was only observed after conditioning the catalyst by equilibrating under reaction conditions for 10 h at 250 °C, and the active surface formed by this conditioning step remained stable even after a 24 h reduction at 300 °C.

Acknowledgements

The authors thank David Ackland for assistance acquiring the catalyst images on the JEOL 2200 FS. Funding for this project was provided by the National Science Foundation (Grant DMR-0506705).

References

- [1] M.D. Amiridis, T. Zhang, R.J. Farrauto, *Appl. Catal. B: Environ.* 10 (1996) 203–227.
- [2] R. Burch, J.P. Breen, F.C. Meunier, *Appl. Catal. B: Environ.* 39 (2002) 283–303.
- [3] A. Fritz, V. Pitchon, *Appl. Catal. B: Environ.* 13 (1997) 1–25.
- [4] F. Garin, *Catal. Today* 89 (2004) 255–268.
- [5] Z.M. Liu, S.I. Woo, *Catal. Rev.* 48 (2006) 43–89.
- [6] Y. Traa, B. Burger, J. Weitkamp, *Micropor. Mesopor. Mater.* 30 (1999) 3–41.
- [7] R.E. Lakis, C.E. Lyman, H.G. Stenger, *J. Catal.* 154 (1995) 261–275.
- [8] R.E. Lakis, Y.P. Cai, H.G. Stenger, C.E. Lyman, *J. Catal.* 154 (1995) 276–287.
- [9] S.H. Oh, J.E. Carpenter, *J. Catal.* 98 (1986) 178–190.
- [10] M.S. Tzou, K. Asakura, Y. Yamazaki, H. Kuroda, *Catal. Lett.* 11 (1991) 33–40.
- [11] Z. Hu, F.M. Allen, C.Z. Wan, R.M. Heck, J.J. Steger, R.E. Lakis, C.E. Lyman, *J. Catal.* 174 (1998) 13–21.
- [12] L. Heezen, V.N. Kilian, R.F. van Slooten, R.M. Wolf, B.E. Nieuwenhuys, in: *Proceedings of the 2nd International Symposium on Catalysis and Automotive Pollution Control*, September 10–13, 1990, Elsevier Science Publ. Co. Inc., New York, NY, USA, Brussels, Belg., 1991, p. 381.
- [13] A.G. Van Den Bosch-Dribergen, M.N.H. Kieboom, A. Van Dreumel, R.M. Wolf, F.C.M.J.M. Van Delft, B.E. Nieuwenhuys, *Catal. Lett.* 2 (1989) 73–79.
- [14] C.E. Lyman, R.E. Lakis, H.G. Stenger, 2nd Mexican Congress of Electron Microscopy, 1994, SSM16.
- [15] C.E. Lyman, R.E. Lakis, H.G. Stenger, *Ultramicroscopy* 58 (1995) 25–34.
- [16] C.E. Lyman, R.E. Lakis, H.G. Stenger, B. Totdal, R. Prestvik, *Mikrochim. Acta* 132 (2000) 301–308.

- [17] D. Gavril, N.A. Katsanos, G. Karaiskakis, *J. Chromatogr. A* 852 (1999) 507–523.
- [18] T. Mailet, J. Barbier, P. Gelin, H. Praliaud, D. Duprez, *J. Catal.* 202 (2001) 367–378.
- [19] F.R. de Boer, *Cohesion in Metals: Transition Metal Alloys*, North-Holland, New York, N.Y., U.S.A, 1988.
- [20] P.A. Dowben, A. Miller, *Surface Segregation Phenomena*, CRC Press, Boca Raton, FL, 1990.
- [21] M. Gruyters, D.A. King, *J. Chem. Soc. Faraday Trans. 93* (1997) 2947–2956.
- [22] Y. Matsumoto, Y. Aibara, K. Mukai, K. Moriwaki, Y. Okawa, B.E. Nieuwenhuys, K. Tanaka, *Surf. Sci.* 377–379 (1997) 32–37.
- [23] C.P. Oliver, B.V. King, D.J. O'Connor, *Surf. Sci.* 561 (2004) 33–42.
- [24] A. Sasahara, H. Tamura, K. Tanaka, *J. Phys. Chem. B* 101 (1997) 1186–1189.
- [25] K. Tanaka, *Surf. Sci.* 357–358 (1996) 721–728.
- [26] K. Tanaka, *Appl. Catal. A: Gen.* 188 (1999) 37–52.
- [27] K. Tanaka, A. Sasahara, *J. Mol. Catal. A* 155 (2000) 13–22.
- [28] P.A.J. Bagot, *Mater. Sci. Technol.* 20 (2004) 679–694.
- [29] P.A.J. Bagot, A. Cerezo, G.D.W. Smith, *Surf. Sci.* 601 (2007) 2245–2255.
- [30] P.A.J. Bagot, A. Cerezo, G.D.W. Smith, T.V. de Bocarme, T.J. Godfrey, *Surf. Interface Anal.* 39 (2007) 172–177.
- [31] P.A.J. Bagot, T.V. de Bocarme, A. Cerezo, G.D.W. Smith, *Surf. Sci.* 600 (2006) 3028–3035.
- [32] A. Bourane, O. Dulaurent, S. Salasc, C. Sarda, C. Bouly, D. Bianchi, *J. Catal.* 204 (2001) 77–88.
- [33] P. Gardner, M. Tüshaus, R. Martin, A.M. Bradshaw, *Surf. Sci.* 240 (1990) 112–124.
- [34] R.J. Gorte, J.L. Gland, *Surf. Sci.* 102 (1981) 348–358.
- [35] G. Pirug, H.P. Bonzel, H. Hopster, H. Ibach, *J. Chem. Phys.* 71 (1979) 593–598.
- [36] W.A. Brown, R.K. Sharma, D.A. King, *J. Phys. Chem. B* 102 (1998) 5303–5308.
- [37] A. Amirnazimi, M. Boudart, *J. Catal.* 39 (1975) 383–394.
- [38] É. Novák, F. Solymosi, *J. Catal.* 125 (1990) 112–122.
- [39] T. Campbell, A.J. Dent, S. Diaz-Moreno, J. Evans, S.G. Fiddy, M.A. Newton, S. Turin, *Chem. Commun.* (2002) 304–305.
- [40] M. Gajdos, J. Hafner, A. Eichler, *J. Phys. Condens. Mater.* 18 (2005) 13–40.
- [41] M. Gajdos, J. Hafner, A. Eichler, *J. Phys. Condens. Mater.* 18 (2005) 41–54.
- [42] F. Garin, *Appl. Catal. A: Gen.* 222 (2001) 183–219.
- [43] W.A. Brown, D.A. King, *J. Phys. Chem. B* 104 (2000) 2578–2595.
- [44] K. Almusaiteer, R. Krishnamurthy, S.S.C. Chuang, *Catal. Today* 55 (2000) 291–299.
- [45] P. Araya, F. Gracia, J. Cortes, E.E. Wolf, *Appl. Catal. B: Environ.* 38 (2002) 77–90.
- [46] D.K. Captain, M.D. Amiridis, *J. Catal.* 184 (1999) 377–389.
- [47] T. Chafik, D.I. Kondarides, X.E. Verykios, *J. Catal.* 190 (2000) 446–459.
- [48] P.T. Fanson, M.R. Horton, W.N. Delgass, J. Lauterbach, *Appl. Catal. B: Environ.* 46 (2003) 393–413.
- [49] E. Fridell, H. Persson, B. Westerberg, L. Olsson, M. Skoglundh, *Catal. Lett.* 66 (2000) 71–74.
- [50] K.I. Hadjiivanov, *Catal. Rev.* 42 (2000) 71–144.
- [51] P.J. Levy, V. Pitchon, V. Perrichon, M. Primet, M. Chevrier, C. Gauthier, *J. Catal.* 178 (1998) 363–371.
- [52] P.B. Rasband, W.C. Hecker, *J. Catal.* 139 (1993) 551–560.
- [53] A. Satsuma, K. Shimizu, *Prog. Energy Combust.* 29 (2003) 71–84.
- [54] W. Schiesser, H. Vinek, A. Jentys, *Appl. Catal. B: Environ.* 33 (2001) 263–274.
- [55] C. Sedlmair, K. Seshan, A. Jentys, J.A. Lercher, *J. Catal.* 214 (2003) 308–316.
- [56] T. Szailer, J.H. Kwak, D.H. Kim, J.C. Hanson, C.H.F. Peden, J. Szanyi, *J. Catal.* 239 (2006) 51–64.
- [57] B. Westerberg, E. Fridell, *J. Mol. Catal. A* 165 (2001) 249–263.
- [58] F. Prinetto, G. Ghiotti, I. Nova, L. Lietti, E. Tronconi, P. Forzatti, *J. Phys. Chem. B* 105 (2001) 12732–12745.
- [59] Y. Su, M.D. Amiridis, *Catal. Today* 96 (2004) 31–41.
- [60] C.L. Levoguer, R.M. Nix, *Surf. Sci.* 365 (1996) 672–682.
- [61] P. Granger, C. Dujardin, J.F. Paul, G. Leclercq, *J. Mol. Catal. A* 228 (2005) 241–253.
- [62] W.S. Epling, L.E. Campbell, A. Yezerets, N.W. Currier, J.E. Parks II, *Catal. Rev.* 46 (2004) 163–245.
- [63] P. Granger, J.P. Dacquin, F. Dhainaut, C. Dujardin, in: P. Granger, V.I. Päravulescu (Eds.), *Past and Present in DeNO_x Catalysis: From Molecular Modelling to Chemical Engineering*, 1st ed., Elsevier, Amsterdam; Boston, 2007, pp. 291–324.
- [64] R. Burch, *Topics Catal.* 24 (2003) 97–102.
- [65] R. Burch, A.A. Shestov, J.A. Sullivan, *J. Catal.* 186 (1999) 353–361.
- [66] F. Dhainaut, S. Pietrzyk, P. Granger, *Appl. Catal. B: Environ.* 70 (2007) 100–110.
- [67] A.A. Shestov, R. Burch, J.A. Sullivan, *J. Catal.* 186 (1999) 362–372.
- [68] J. Shibata, M. Hashimoto, K. Shimizu, H. Yoshida, T. Hattori, A. Satsuma, *J. Phys. Chem. B* 108 (2004) 18327–18335.
- [69] W.C. Hecker, A.T. Bell, *J. Catal.* 92 (1985) 247–259.